JYX
JYVÄSKYLÄN YLIOPISTO
UNIVERSITY OF JYVÄSKYLÄ

This is a self-archived version of an original article. This version may differ from the original in pagination and typographic details.

Author(s): Broas, Mikael; Lemettinen, Jori; Sajavaara, Timo; Tilli, Markku; Vuorinen, Vesa; Suihkonen, Sami; Paulasto-Kröckel, Mervi

Title: In-situ annealing characterization of atomic-layer-deposited Al2O3 in N2, H2 and vacuum atmospheres

Year: 2019

Version: Accepted version (Final draft)

Copyright: © 2019 Published by Elsevier B.V.

Rights: CC BY-NC-ND 4.0

Rights url: https://creativecommons.org/licenses/by-nc-nd/4.0/

Please cite the original version:

Broas, M., Lemettinen, J., Sajavaara, T., Tilli, M., Vuorinen, V., Suihkonen, S., & Paulasto-Kröckel, M. (2019). In-situ annealing characterization of atomic-layer-deposited Al2O3 in N2, H2 and vacuum atmospheres. Thin Solid Films, 682, 147-155. https://doi.org/10.1016/j.tsf.2019.03.010

Accepted Manuscript

In-situ annealing characterization of atomic-layer-deposited Al2O3 in N2, H2 and vacuum atmospheres

Mikael Broas, Jori Lemettinen, Timo Sajavaara, Markku Tilli, Vesa Vuorinen, Sami Suihkonen, Mervi Paulasto-Kröckel

PII: S0040-6090(19)30153-1
DOI: https://doi.org/10.1016/j.tsf.2019.03.010
Reference: TSF 37198

To appear in: *Thin Solid Films*

Received date: 3 July 2018
Revised date: 3 March 2019
Accepted date: 12 March 2019

Please cite this article as: M. Broas, J. Lemettinen, T. Sajavaara, et al., In-situ annealing characterization of atomic-layer-deposited Al2O3 in N2, H2 and vacuum atmospheres, Thin Solid Films, https://doi.org/10.1016/j.tsf.2019.03.010

This is a PDF file of an unedited manuscript that has been accepted for publication. As a service to our customers we are providing this early version of the manuscript. The manuscript will undergo copyediting, typesetting, and review of the resulting proof before it is published in its final form. Please note that during the production process errors may be discovered which could affect the content, and all legal disclaimers that apply to the journal pertain.

ACCEPTED MANUSCRIPT

In-situ annealing characterization of atomic-layer-deposited Al_2O_3 in N_2, H_2 and vacuum atmospheres

Mikael Broas[a)]

Aalto University, Department of Electrical Engineering and Automation, P.O. Box 13500, FIN-00076, Aalto, Espoo, Finland

Jori Lemettinen

Aalto University, Department of Electronics and Nanoengineering, P.O. Box 13500, FIN-00076, Aalto, Espoo, Finland

Timo Sajavaara

University of Jyväskylä, Department of Physics, Jyväskylä, P.O. Box 35, FIN-40014, Finland

Markku Tilli

Okmetic Oy, Piitie 2, 01510 Vantaa, Finland

Vesa Vuorinen

Aalto University, Department of Electrical Engineering and Automation, P.O. Box 13500, FIN-00076, Aalto, Espoo, Finland

Sami Suihkonen

Aalto University, Department of Electronics and Nanoengineering, P.O. Box 13500, FIN-00076, Aalto, Espoo, Finland

Mervi Paulasto-Kröckel

ACCEPTED MANUSCRIPT

ACCEPTED MANUSCRIPT

Aalto University. Department of Electrical Engineering and Automation, P.O. Box 13500, FIN-00076, Aalto, Espoo, Finland

[a] Electronic mail: mikael.broas@aalto.fi

Atomic-layer-deposited Al_2O_3 films can be used for passivation, protective, and functional purposes in electronic devices. However, as-deposited, amorphous alumina is susceptible to chemical attack and corrosion during manufacturing and field-use. On the contrary, crystalline Al_2O_3 is resistant against aggressive chemical treatments and corrosion. Here, high-temperature treatments in N_2, H_2, and vacuum were used to crystallize alumina which exhibited different crystalline phases. The annealing process was monitored continuously in situ by measuring the film temperature and surface reflectance to understand the crystallization kinetics. Ex-situ x-ray diffraction, electron microscopy, and composition analysis were used to probe the structure of the crystallized films and explain the formation of different alumina phases. This study provides a set of boundary conditions, in terms of temperature and atmosphere, for crystallizing chemically stable atomic-layer-deposited alumina for applications requiring a film thickness in the range of tens of nanometers without defects such as cracks.

Keywords: Atomic layer deposition; Aluminum oxide; barrier film; high-temperature annealing; crystallization

1. INTRODUCTION

Atomic-layer-deposited (ALD) thin films are ideal for applications that require thin, uniform coatings that cover even the most challenging high aspect ratio structures and other demanding geometries. Furthermore, the precise thickness control of ALD films enables them to be used in nanoelectronics fabrication where the ever-decreasing dimensions require sub nanometer

ACCEPTED MANUSCRIPT

ACCEPTED MANUSCRIPT

thickness control over large areas. Many ALD films are amorphous in the as-deposited state [1], which can be beneficial in some applications [2,3], but can render the films unstable in demanding environments such as during high-temperature processing [4], or aggressive chemical treatments such as the Radio Corporation of America (RCA) cleaning [5]. Furthermore, the effects of deliberate or process-related crystallization of amorphous films during high-temperature processing need to be controlled to achieve the desired electrical properties in applications such as gate oxides.[3,6–8] Therefore, understanding the crystallization process of an amorphous film is of high importance regardless whether the crystallization process is deliberate or a consequence of additional processing steps.

Crystallizing any film with as much control as possible of the final structure has at least three challenges. First, determining the crystallization temperature accurately can be challenging since most annealing equipment lack in-situ measurement capabilities. Second, the thermal budget of multimaterial structures may impose limitations and, therefore, a temperature that is known to be clearly higher than the expected crystallization point (‘play it safe’ approach) may not be utilized. Third, materials that show polymorphism may change their structure with higher temperatures above the crystallization point, while ex-situ data does not provide accurate information of the transition points. Nevertheless, crystallized ALD Al_2O_3 films for barrier applications have been demonstrated to be stable in a variety of chemical solutions and to provide excellent impermeability against gases [9–11]. On the contrary, as-deposited, amorphous ALD Al_2O_3 shows poor stability in many chemical solutions including water [9,12,13]. However, ALD Al_2O_3 that has been crystallized close to the amorphous-crystalline transition temperature has also showed instability in SC-1 and HF after 60 minutes of exposure [5]. Perhaps the most characterized ALD material to undergo high-temperature processing is HfO_2, and its derivatives such as HfON and

ACCEPTED MANUSCRIPT

HfSiON, utilized in complementary metal-oxide-semiconductor (CMOS) technologies as the gate oxide. As such, the behavior of HfO-based films need to be predictable during high-temperature processing and many studies exist on the topic.[3,6–8,14] For example, ALD HfO_2 has been studied with differential scanning calorimetry (DSC) to accurately find the crystallization point in-situ [15]. In addition, post-annealing x-ray diffraction (XRD) studies have been conducted on HfO_2 films to iterate the crystallization point and to deduct the crystal structure of HfO_2 films deposited at different temperatures [6]. The HfO_2 films in [6] crystallized into the monoclinic phase when starting from amorphous films deposited at 200 °C but exhibited crack-liked voiding. The films deposited at an above 300 °C were a mixture of tetragonal and monoclinic phases and transformed fully into the monoclinic phase also after high-temperature annealing but did not exhibit cracking. Finally, the crystallization kinetics of ALD HfO_2 has been studied in-situ using transmission electron microscopy (TEM) [7].

Contrary to ALD HfO_2, few high-temperature processing -focused studies on ALD Al_2O_3 exist despite the importance of crystallizing Al_2O_3 films to tailor their functional properties, and chemical and thermal stability.[16–18] Moreover, depositing polycrystalline Al_2O_3 with thermally-activated ALD requires temperatures above 600 °C typically not achieved by many ALD reactors [19]. Furthermore, no in-situ studies exist for observing the crystallization of ALD Al_2O_3 although the interfacial behavior of very thin (some nm) ALD Al_2O_3 on Si has been observed in-situ with TEM [20]. Furthermore, the onset of crystallization may change as a function of the film thickness. For example, Jakschik et al.[16] studied alumina films of a few nm and found the crystallization of ALD Al_2O_3 to begin at temperatures well above 800 °C, whereas thicker ALD alumina films have been demonstrated to crystallize at 800 °C [5]. The differences may arise from the original stoichiometry, impurities, the utilized atmosphere, or from the thicknesses of the films

ACCEPTED MANUSCRIPT

influencing the number of suitable nucleation centers. The goal of this study is to investigate the crystallization behavior of 'thick' - 100 nm - ALD Al_2O_3 on Si for applications such as barriers. The results are divided into two parts. First, the quality of the as-deposited material is investigated using TEM and time-of-flight elastic recoil detection analysis (ToF-ERDA). The goal is to start from high quality material to exclude film properties that could affect the crystallization and final microstructure such as poor stoichiometry or a high level of impurities. Second, the crystallization temperature is determined in situ by observing the reflectance of the films. Furthermore, the wafer curvature data is collected in situ to understand the stress development in the films during the annealing and crystallization. In addition, different atmospheres are used to investigate their effect on the onset of the crystallization and phase transformations of alumina which can manifest various metastable transition phases. The used atmosphere can have a significant effect on the film properties [21,22].

2. EXPERIMENTAL

ALD alumina films were dual-side deposited in a thermal process in a batch reactor (Beneq P400A) on a full cassette of 25 Si (100) single-side-polished wafers. The silicon wafers were with their native oxide. Trimethylaluminum (TMA) was used as the Al source, while the second precursor – the oxygen source – was H_2O vapor. A purge cycle was applied between the half reactions. The deposition temperature was 450 °C. All films were visually inspected for obvious defects and color variation. One wafer with the as-deposited film was measured with an ellipsometer (Plasmos SD2300) at the wavelength of 632.8 nm and an angle of incidence of 70°. In addition, selected samples (as-deposited and annealed) were characterized for structures with

ACCEPTED MANUSCRIPT

ACCEPTED MANUSCRIPT

TEM (JEOL JEM-2800 and JEM-2200FS) at 200 kV, and for elemental depth profiles with ToF-ERDA using 10.5 MeV and 11.9 MeV ^{63}Cu ions [23].

The films were annealed in a metal-organic vapor phase reactor (MOVPE, Aixtron CS18350) with 1×6-inch close coupled shower-head configuration. 99.9999% pure N_2 and H_2 were used as the ambient gases. Table 1 presents the used annealing parameters. Heating and cooling rates were 0.2 °C/s and 0.7 °C/s, respectively, for all the MOVPE annealing experiments. The sample surface temperature, the sample reflectance at 405 nm, and the sample curvature were measured optically in situ. A 405-nm wavelength laser was focused in normal incidence on the wafer through one of the view-ports of the reactor for the reflectance measurements. Wafer surface temperature measurements with emissivity correction were conducted similarly. First, the sample reflectivity was measured in the infra-red region. Then, the sample blackbody radiation was measured. These two measurements were used together with Planck's law to estimate the sample surface temperature. For the wafer curvature measurements, a second 405-nm laser setup, consisting of two parallel beams, was focused on the sample surface. The deviation of the beams reflected from the sample was then converted to curvature estimates. In addition, high vacuum (HV) annealing ($p_{tot} < 10^{-4}$ Pa) was conducted on two films in a furnace (Webb Red Devil M) (Table 1 bottom row). The ramp rate in the HV experiments was likewise 0.2 °C/min and cooling was achieved through natural heat dissipation.

TABLE 1. The annealing target wafer surface temperatures, hold times at the annealing temperatures, pressures, and annealing atmospheres.

Sample	Target wafer surface temperature (°C)	Hold time (min)	Pressure (Pa)	Ambient

ACCEPTED MANUSCRIPT

Alumina 1 & 5	1300	30	10^5	N_2
Alumina 2 & 6	1300	30	10^5	H_2
Alumina 3 & 7	1300	30	1000	N_2
Alumina 4 & 8	1300	30	1000	H_2
Alumina 9	950	0	10^5	N_2
Alumina 10	950	0	10^5	H_2
Alumina 11	950	0	1000	N_2
Alumina 12	950	0	1000	H_2
Alumina 13	800	30	10^5	N_2
Alumina 14	800	30	10^5	H_2
Alumina 15	1200	30	10^5	H_2
Alumina 16 & 17	1000	60	$<10^{-4}$	HV

All samples were characterized with optical microscopy and one of each repetition (samples 5–8 and 17) together with the single-experiment samples (9–15) with XRD. Symmetrical θ-2θ XRD analyses were carried out with an x-ray diffractometer (Rigaku SmartLab) equipped with a 9 kW rotating Cu anode source. The incident beam was monochromatized using a multilayer mirror and a Ge (220) double bounce monochromator. Indexing was based on data from the in Inorganic Crystal Structure Database (ICSD).

3. RESULTS

ACCEPTED MANUSCRIPT

ACCEPTED MANUSCRIPT

3.1 As-deposited ALD Al_2O_3

The growth per cycle (GPC) of the films, measured from one wafer, was 0.07 nm, non-uniformity 1%, thickness 101 ± 1 nm, and the refractive index 1.66. The GPC was lower compared to the GPC of a saturated TMA-H_2O process at 300 °C which lies between 0.08 and 0.1 nm/cycle [10,24]. It is noteworthy that TMA begins to decompose at approximately 370 °C which could induce chemical vapor deposition type film growth [25]. Regardless, the increased temperature decreases the concentration of reactive OH groups at the surface of Al_2O_3 which in fact hinders the GPC [24]. More information of the as-deposited Al_2O_3 films can be found in Ref. [5]. The as-deposited films were found amorphous (Fig. 1). No Si native oxide was seen in the high-resolution TEM (HRTEM) images. The native oxide has likely reacted with the reducing TMA during the deposition.

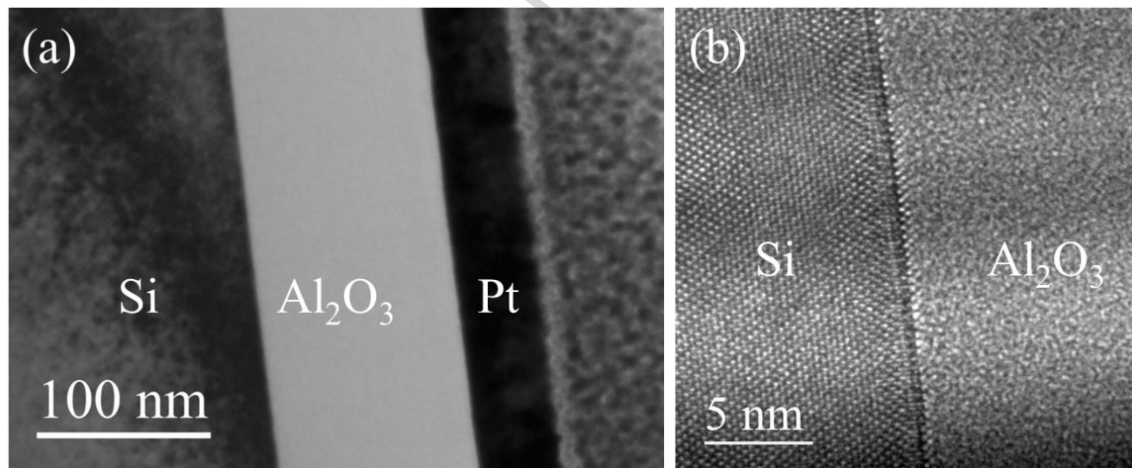

FIG. 1. TEM images of the as-deposited Al_2O_3 film. (a) A bright-field image taken with only the zero-order beam selected, and (b) the HRTEM image show that the as-deposited films were amorphous. No Si native oxide was detected during the high-resolution imaging.

ACCEPTED MANUSCRIPT

The chemical composition of the as-deposited films was characterized with ToF-ERDA which showed the bulk of the films to be stoichiometric and almost free of impurities (Fig 2.). Similar impurity levels are achieved with TMA-H_2O-based deposition at 250 °C with the hydrogen and carbon concentrations being 1 at.% and <0.2 at.%, respectively [26].

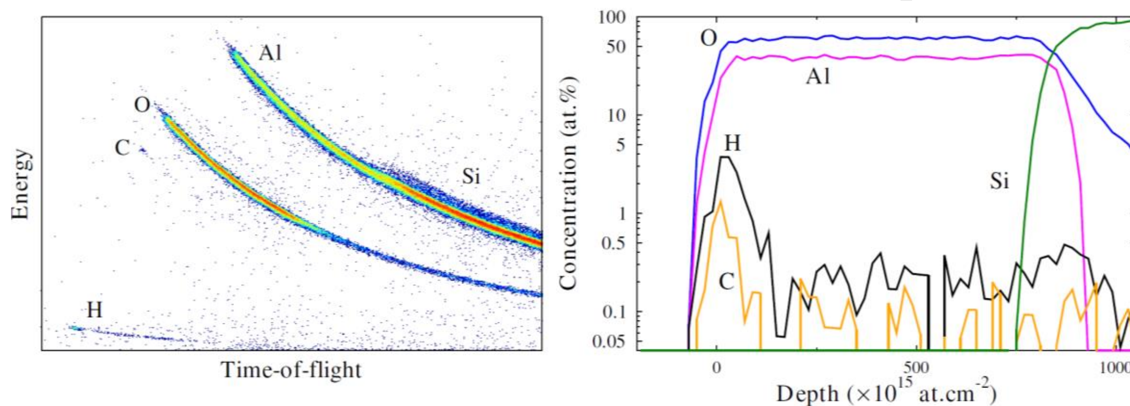

FIG. 2. The ToF-E histogram and corresponding depth ToF-ERDA depth profiles of the as-deposited Al_2O_3 film on Si. The Al and Si signals cannot be entirely separated at the interface. Note that the y-axis is logarithmic.

Therefore, the starting material for the annealing experiments was high-purity, amorphous ALD Al_2O_3 with no obvious native oxide or other reaction layers at the Al_2O_3-Si interface.

3.2 In-situ reflectance and wafer curvature

Figure 3 presents the film reflectance at 405 nm during the annealing plotted against sample surface temperature in 10^5 Pa N_2, 10^5 Pa H_2, 1000 Pa N_2, and 1000 Pa H_2 ambients. A temperature ramp from room temperature to the thermocouple set-point of 1490 °C was applied with a temperature ramp rate of 0.2 °C/s. The annealing in each ambient was repeated twice and identical results were observed. For all samples, a clear drop in the reflectance can be seen at about 850 °C

ACCEPTED MANUSCRIPT

(Fig. 3, Transition 1). This change in the reflectance is a clear indication of a physical change in the films implying a transition in the film crystalline structure. A thin layer composed of Al, Si, and O is expected to grow between the film and the substrate, but its effect is expected to be minimal due to its thickness compared to the total film thickness. The noise in the 10^5 Pa N_2 annealing reflectance curve is due to increased wafer curvature. A second, more moderate change is observed near 1000 °C (Fig. 3, Transition 2), indicated by a change in the slope of the reflectance. The films which were annealed in 10^5 Pa N_2, 1000 Pa N_2, and 1000 Pa H_2 reached a surface temperature of 1160 °C, 1120 °C, and 1100 °C, respectively. The differences in the final temperatures are due to the cooling effect of the annealing ambient. In contrast, the film annealed in 10^5 Pa H_2 reached 1300 °C and exhibited two additional reflectance changes (Fig. 3, Transition 3 and 4). The third transition occurs at 1150 °C which is visible as a change in the reflectance slope from positive to negative. The last observed change had the most pronounced effect on the sample reflectance. Visual inspection revealed that the film color had changed drastically.

ACCEPTED MANUSCRIPT

ACCEPTED MANUSCRIPT

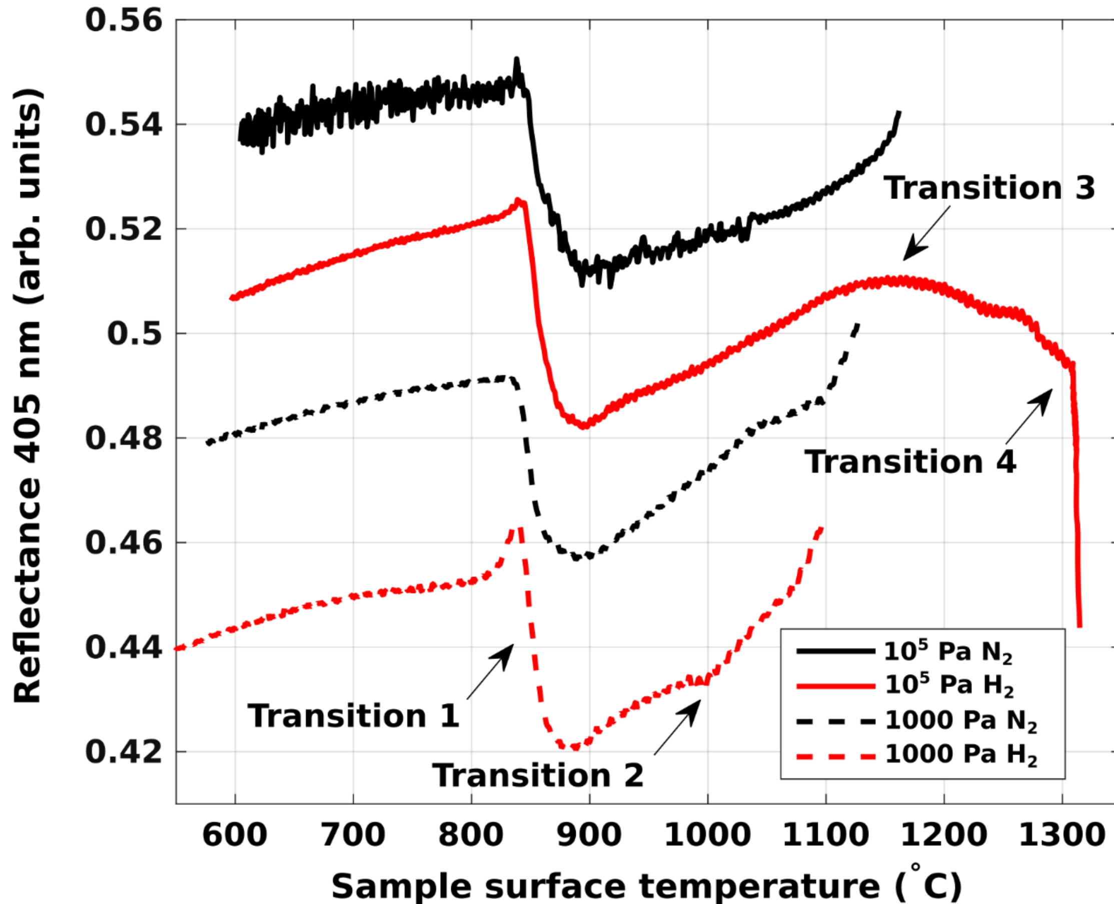

FIG. 3. Surface reflectances at 405 nm plotted against film surface temperature during the annealing in 10^5 Pa N_2 (solid black), 10^5 Pa H_2 (solid red), 1000 Pa N_2 (dashed black), 1000 Pa H_2 (dashed red) ambients. The curves have been offset for readability.

Figure 4 presents the changes in the curvatures of the double-side Al_2O_3-coated wafers during the annealing plotted against film surface temperature in 10^5 Pa N_2, 10^5 Pa H_2, 1000 Pa N_2, and 1000 Pa H_2 ambients. The continuous slope is caused by the difference in the coefficients of thermal expansion (CTE) of the silicon wafer and the alumina in addition to a thermal gradient between the wafer backside and surface. Considering purely the CTE mismatches ($CTE_{Al2O3} > CTE_{Si}$) means that during heating the alumina film will be in compressive stress [27]. After the cooling, at room temperature, crystallized ALD alumina films are expected to be under tensile stress [10].

ACCEPTED MANUSCRIPT

The thermal gradient originates from the heated susceptor and cooling effect of the process gas flow. As the susceptor temperature is increased, the thermal gradient increases which causes concave wafer bow and compressive in-plane film stress on top of the wafer. The slope of the curvature for the film annealed in 10^5 Pa N_2 is extremely high and the film cracks completely at 1250°C (Fig. 4 inset). This behavior is not fully explained by thermal expansion. The curvature and the resulting film mechanical stress are directly proportional to the vertical temperature gradient over the wafer and the film [28]. Although the heat transfer of 10^5 Pa N_2 is greater than in the other atmospheres, the resulting difference in the temperature gradient is small compared to 10^5 Pa H_2. In fact, using a different pressure has a greater effect on the sample surface temperature than the process gas itself (Fig. 5). That is, Figure 5 shows that the surface temperatures for the 10^5-Pa atmospheres rise faster than the 1000-Pa atmospheres.

The crystalline transition at 850 °C visible in the film reflectance data of Figure 3 does not change the wafer curvature slopes significantly. Therefore, the crystalline transition does not strongly alter the film stress. In contrast, the second change occurring near 1000 °C clearly reduces the wafer curvature, and thus, suggest that some amount of the film stress is relaxed during this change. In addition, discontinuities in the curvature data also suggest crack formation during the second change for samples annealed in 1000 Pa N_2 and 1000 Pa H_2 ambients (Fig. 4). The third and fourth changes in reflectance (Fig. 3), occurring only for the sample in 10^5 Pa H_2 ambient, do not have a clear effect on the wafer curvature, and thus, do not significantly alter the film stress.

ACCEPTED MANUSCRIPT

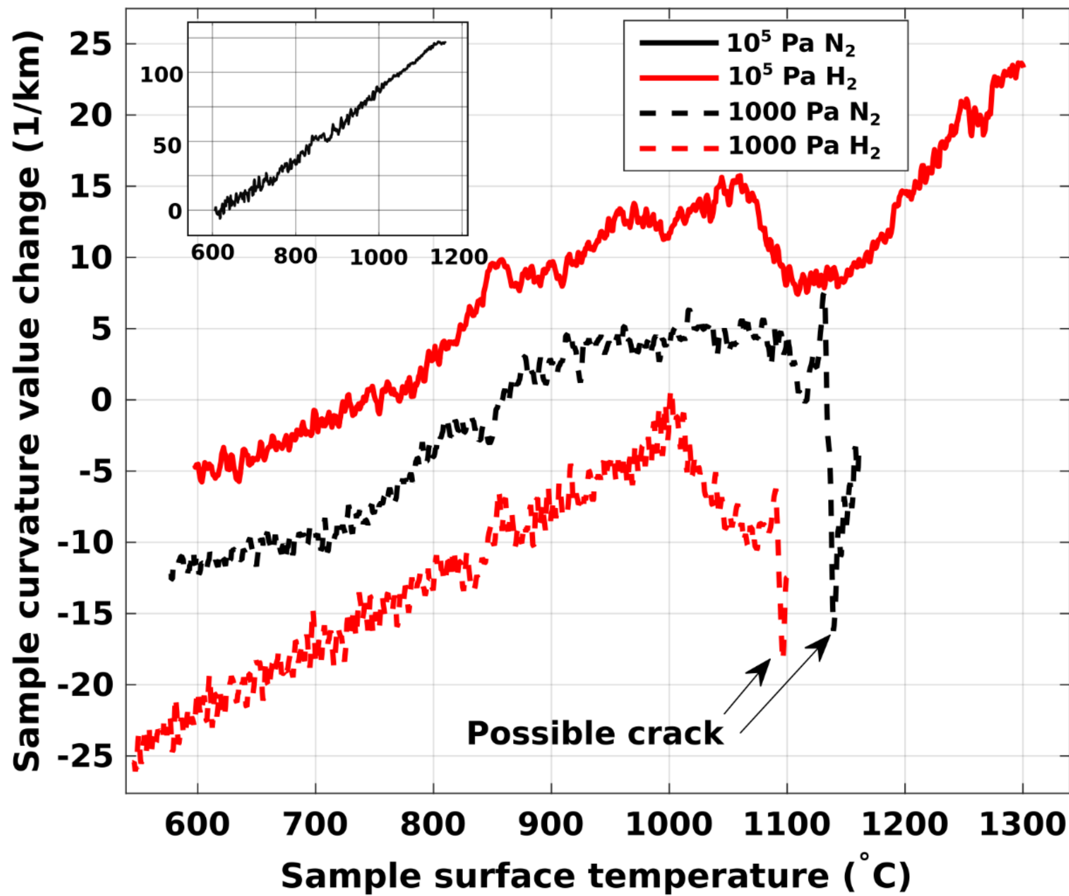

FIG. 4. Sample curvature value changes plotted against sample surface temperatures during the annealing in 10^5 Pa N_2 (solid black), 10^5 Pa H_2 (solid red), 1000 Pa N_2 (dashed black), and 1000 Pa H_2 (dashed red). The curves have been offset for readability. Note that the curvature for the wafer annealed under 10^5 Pa N_2 is presented in the inset due to different axes. Two temperatures have been indicated for samples annealed under 1000 Pa N_2 and 1000 Pa H_2 where a discontinuity in the curvature value suggests crack formation.

Four samples were annealed up to 950 °C nominal (reactor setpoint) film surface temperatures in the four previously used ambients: 10^5 Pa N_2, 10^5 Pa H_2, 1000 Pa N_2, 1000 Pa H_2. The goal was to study the crystalline transition indicated by the clear drop in reflectance. After reaching 940 °C

ACCEPTED MANUSCRIPT

(realized temperature at the setpoint), the samples were cooled back to room temperature to freeze the crystalline structures. Figure 5 presents the reflectance and film surface temperature measurements. The films underwent the crystalline transition occurring near 850 °C (Fig. 5). The differences in sample temperatures against time are due to the different cooling effects of the annealing ambients. The annealing ambient does not significantly alter the duration of the crystalline transition as indicated by the similar durations of the reflectance changes.

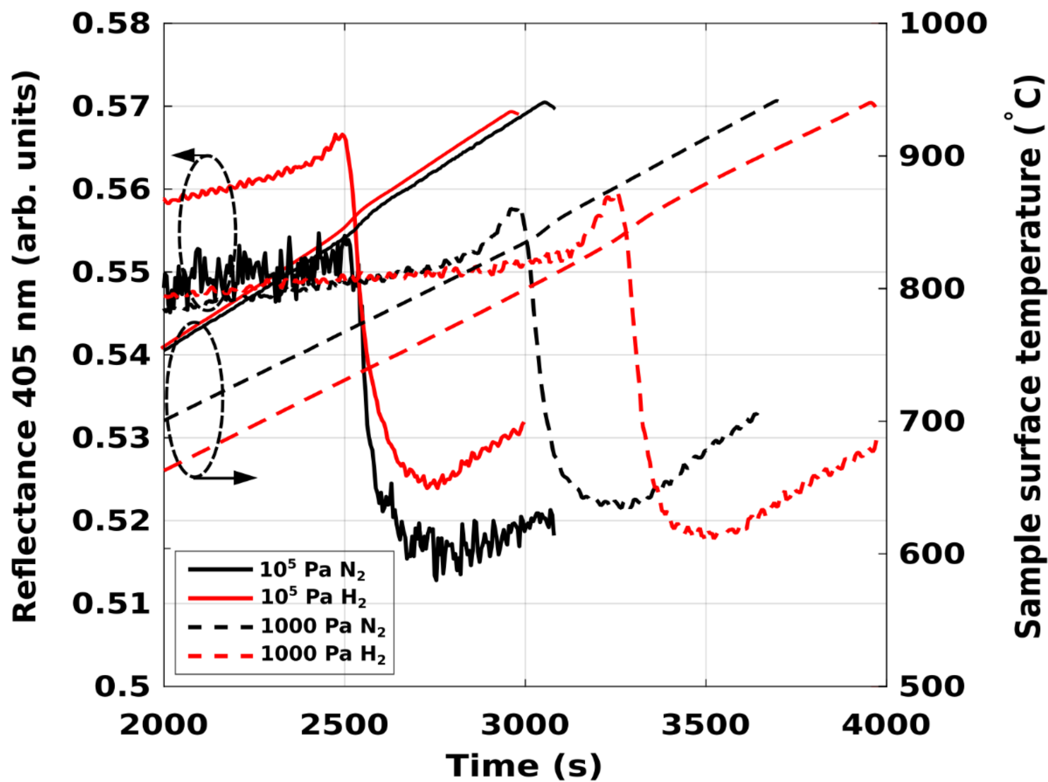

FIG. 5. Surface reflectance at 405 nm and surface temperature during annealing in 10^5 Pa N_2 (solid black), 10^5 Pa H_2 (solid red), 1000 Pa N_2 (dashed black), 1000 Pa H_2 (dashed red) up to 940 °C. After reaching 940 °C each film was cooled back to the room temperature to freeze the first resulted phases as opposed to the experiments in Figure 3.

ACCEPTED MANUSCRIPT

Two films were annealed up to 800 °C nominal film surface temperature in 10^5 Pa N_2 and 10^5 Pa H_2 to study the kinetics of the first transition. The annealing temperature was held for 30 minutes before cooling the samples back to room temperature (Fig. 6). Note that the differences in the sample cooling caused by the annealing ambients together with the differences in wafer curvature caused the samples to reach different surface temperatures with the same temperature set-point. Thus, the crystallization incubation times cannot be explicitly compared in these atmospheres. Nevertheless, Figure 6 shows that the transition does not occur immediately after reaching 810 °C temperature (Fig. 6). It takes about 1000 s for the reflectance to change significantly in the case of the 10^5 Pa H_2 atmosphere. Furthermore, the rate of change in reflectance is slower compared to the annealing conducted up to 940 °C in Figure 5, where the change from the reflectance of 0.56 to below 0.53 takes about 100 s compared to the 500 s for a similar change in Figure 6.

ACCEPTED MANUSCRIPT

ACCEPTED MANUSCRIPT

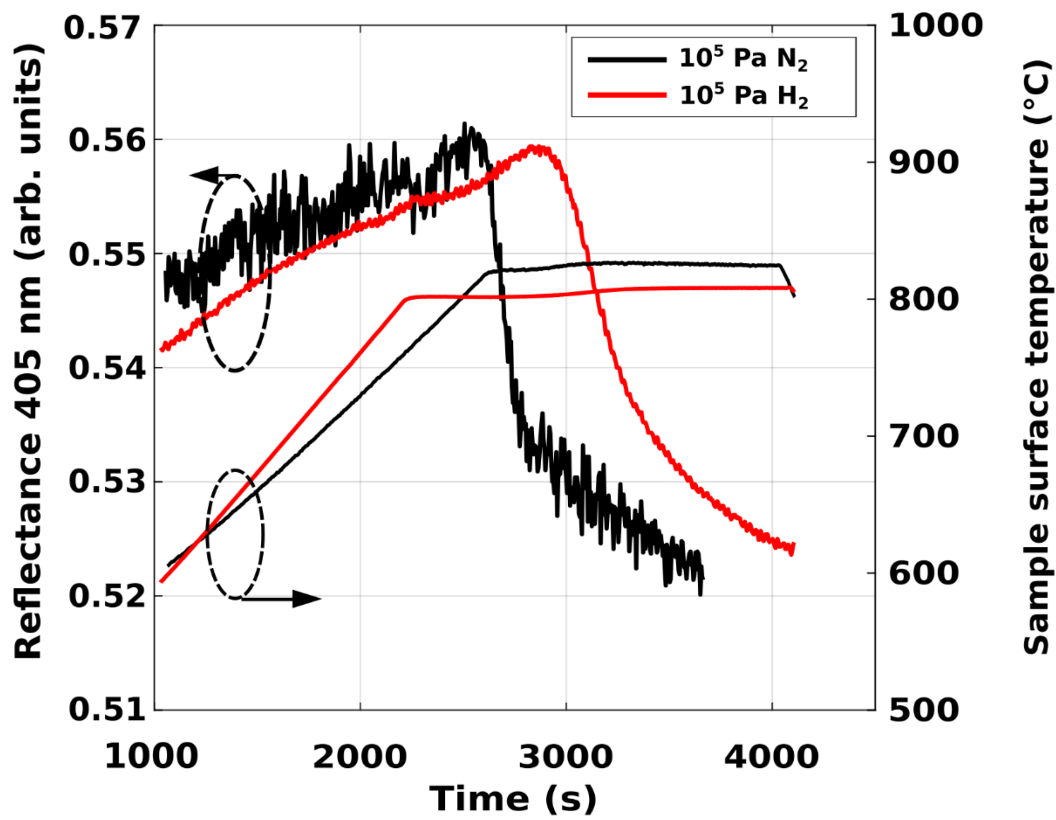

FIG. 6. Reflectance at 405 nm and surface temperature during annealing in 10^5 Pa N_2 and 10^5 Pa H_2 up to 826 °C and 809 °C, respectively. The temperatures were maintained for 30 minutes.

To study the third change where the reflectance started to drop in Figure 3, a film was annealed at 1190 °C nominal substrate surface temperature for 30 minutes under 10^5 Pa H_2. Figure 7 presents the sample reflectance at 405 nm and surface temperature measurement for 10^5 Pa H_2. The annealing run up to 1300 °C from Figure 3 is provided as a comparison. The sample undergoes the crystalline transition (drop in reflectance) and the second change (change in the slope of reflectance) at about 850 °C and 1000 °C, respectively (Fig. 7). The third change (gradual drop in reflectance) occurs almost immediately after reaching 1190 °C. The sample does not undergo the fourth change where the reflectance dropped drastically (visible in Fig. 3).

ACCEPTED MANUSCRIPT

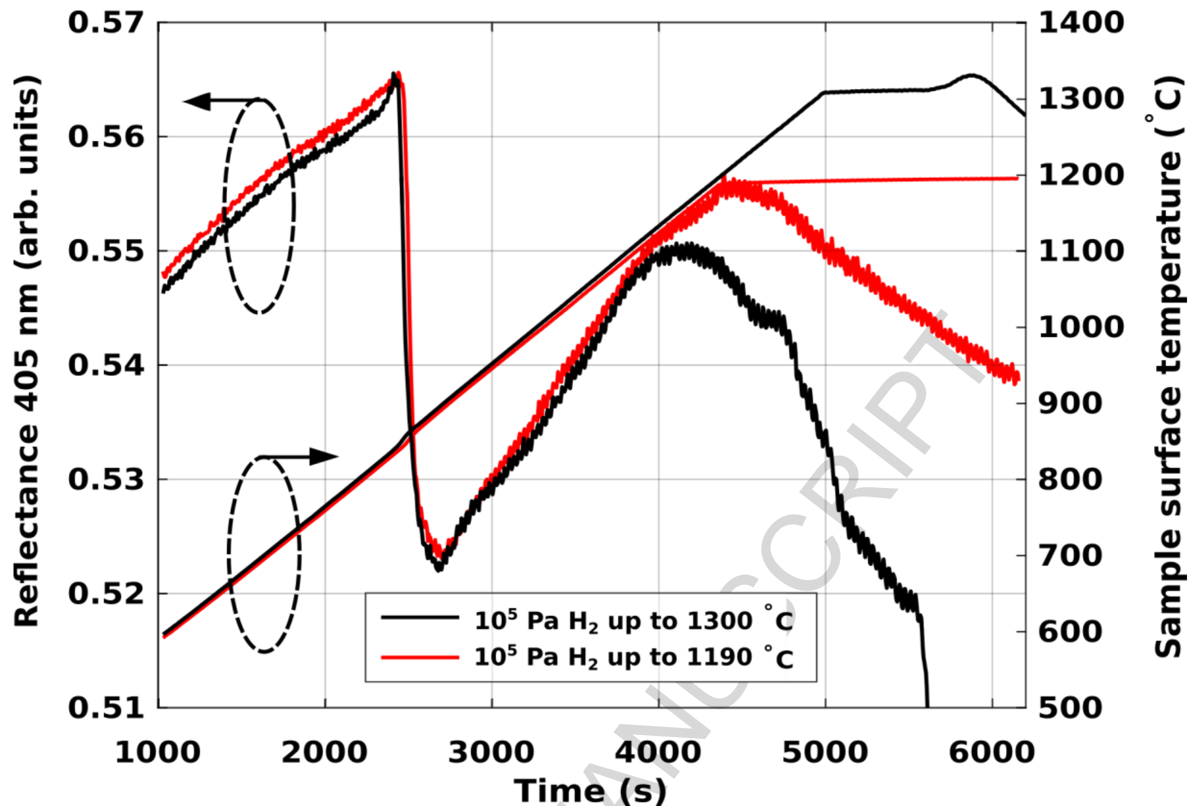

FIG. 7. Reflectance at 405 nm and surface temperature during annealing in 10^5 Pa H_2 up to 1190 °C and up to 1300 °C film surface temperatures represented by the red and black curves, respectively. The temperatures were maintained for 30 minutes.

3.3 Appearance, structure, and chemical composition

The films were characterized after the annealing treatments for visual appearance, structure, and chemical composition. Figure 8 presents the representative optical micrographs of the films. Cracks were present in the MOVPE annealing films where the target temperature was 1200 °C, or 1300 °C and the film color did not change drastically (Alumina 1, 3–5, 7–8, and 15). The 10^5 Pa H_2 samples that were annealed up to 1300 °C – Alumina 2 and 6 – changed their color drastically (Fig. 8b). These samples, i.e., Alumina 2 and 6, did not display cracks in either the optical imaging

ACCEPTED MANUSCRIPT

or wafer curvature data. The vacuum-annealed films exhibited blistering (Fig. 8c) and were more closely characterized in [29]. The films 9–14 did not show visual defects.

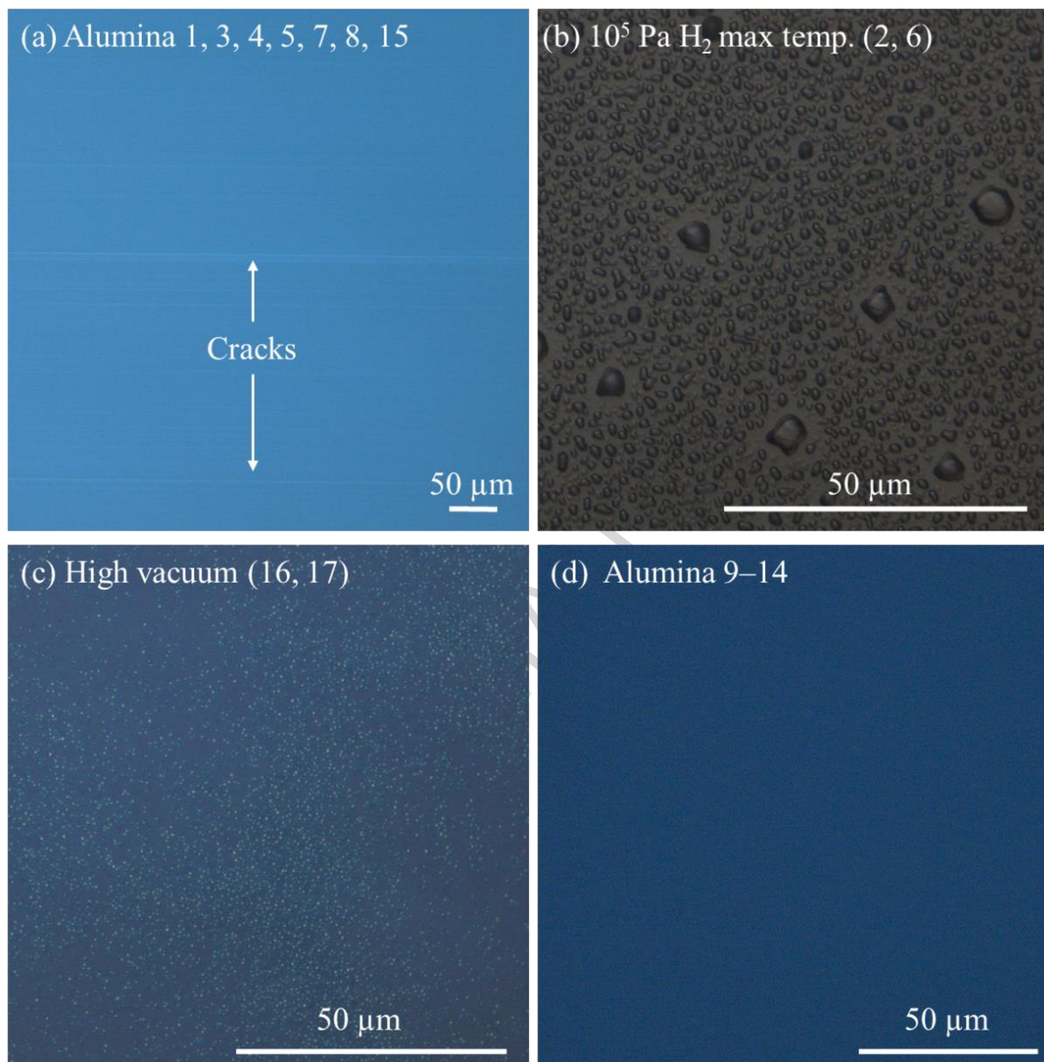

FIG. 8. Optical micrographs of annealed ALD Al_2O_3 films. (a) Cracks were visible in films Alumina 1, 3-5, 7-8, and 15. (b) The surface morphology and color drastically changed due to the annealing in films Alumina 2 and 6. (c) High vacuum annealing at 1000 °C induced blisters to the films. (d) No defects were present in films 9–14 and as-deposited films. Note that the shade of the blue in images (a), (c), and (d) differs mainly due to the different digital contrasts to highlight the defects.

ACCEPTED MANUSCRIPT

The annealing (MOVPE in situ annealing and HV annealing) and the visual inspection results are summarized in Table 2.

TABLE 2. Summary of the samples. 'Max temperature' refers to the data in Figures 3 and 4, 'Freeze first resulting phase' to Figure 5, 'Kinetics' to Figure 6, and 'Higher order transformations' to Figure 7.

Sample	Atmosphere	Reached peak temperature (°C)	Type of experiment	Visual inspection
Alumina 1 & 5	10^5 Pa N_2	1160	Max temperature	Cracks
Alumina 2 & 6	10^5 Pa H_2	1300	Max temperature	Change in color and morphology
Alumina 3 & 7	1000 Pa N_2	1120	Max temperature	Cracks
Alumina 4 & 8	1000 Pa H_2	1100	Max temperature	Cracks
Alumina 9-12	The atmospheres as above (e.g. 9 in 10^5 Pa N_2)	940	Freeze first resulting phase	No cracks
Alumina 13	10^5 Pa N_2	826	Kinetics	No cracks
Alumina 14	10^5 Pa H_2	809	Kinetics	No cracks
Alumina 15	10^5 Pa H_2	1190	Higher order transformations	Cracks
Alumina 16 & 17	High vacuum	1000	Blister investigation	Blisters

Phase and structural analyses of the films were carried out with ex-situ XRD and TEM characterization. Figure 9 presents the XRD data of the films 5–15, one HV, and one as-deposited film. Note that the films 5–8 were duplicates of the films 1–4 where the MOVPE in-situ data was identical for both the original and the duplicated experiment. Furthermore, an as-deposited film

ACCEPTED MANUSCRIPT

and N_2-annealed films deposited with the same ALD reactor and recipe have been previously characterized in [5] and a HV-annealed film in [29]. The XRD results presented here, conducted on a different batch of wafers, coincide with the previous results. The XRD results can be divided into two distinct observations related to the phase analysis and crystalline quality.

First, the MOVPE reflectance data showed a clear transition above 800 °C and other more discrete changes above 1000 °C (Fig. 3). However, the diffractograms (Fig. 9) indicate the same θ phase for the films 5, 7–15 meaning that no additional phase transformations took place at the higher temperatures [30]. Film Alumina 6, one that showed a drastic change in its visual appearance, does not show crystalline alumina XRD peaks. Likewise, the as-deposited film did not show alumina-related XRD peaks as expected (amorphous structure). The HV-annealed film, on the other hand, has a clearly deviating diffractogram best indexed with α and κ indexing [31,32]. A different scaling used in [29] showed in addition θ peaks which were visible in the XRD data examined here also with a different scaling (data not shown). Furthermore, many peaks present in the powder spectra, including some stronger peaks, are not present in Figure 9 indicating the films to have crystallized with a preferential orientation. Indeed, additional TEM images in [5] and [29] show preferential orientation of the crystallized grains in similar films. All indexing data were obtained from the Inorganic Crystal Structure Database (ICSD) while the Si (002) reflection was calculated from the Si unit cell (a = 0.5431 nm) with the Cu K-α_1 radiation (0.1541 nm wavelength). Figure 10 presents the HRTEM and fast Fourier transform (FFT) images of a N_2-annealed Al_2O_3 film from the study in [5] where the best indexing was obtained with pure θ-Al_2O_3, and HV-annealed film from [29] where the best indexing was obtained with a combination of θ, κ, and α. The TEM images also support the notion that the microstructures and phases of the films with congruent

ACCEPTED MANUSCRIPT

XRD indexing (bare θ vs. mixed indexing) differ from each other. Note that the θ peaks of the HV-annealed film are not visible due to the scaling of Figure 9 to accommodate all the data.

Second, the higher annealing temperatures increase the intensities and decrease the widths of the XRD peaks. Increased intensity and decreased width of a diffraction peak indicated improved crystalline quality (grain size and crystallized fraction). Films 13 and 14 induced the lowest intensities and broadest peaks as expected because the aim of the 'Kinetic investigations' was to find out the crystallization points and compare whether the atmospheres play any role in that. Therefore, the reactor temperature was low compared to the other experiments. The crystallization kinetics depend on the temperature meaning that the crystallized fraction and grain size end up being the smallest in films 13 and 14 also indicated by the XRD analysis. However, because the different atmospheres induced different heating environments in the reactor it is challenging to obtain the exact same peak temperatures. The crystalline quality improves as the annealing temperature has been increased (Alumina 5, 7, 8, 15) to above 1000 °C though these films also exhibited cracks (Fig. 8). Films 9–12 have crystalline quality somewhere between the above-mentioned films.

The Si (002) peaks align with each other in all the samples except for Film 5 (10^5 Pa N_2 maximum temperature). Furthermore, the θ ($20\bar{1}$) reflection has also displaced to a lower 2θ value in Film 5. The XRD scan has been taken in the symmetrical θ-2θ geometry measuring lattice planes that lie in-plane with respect to the substrate. A shift towards smaller 2θ values means a larger distance between lattice planes indicating in-plane compression of the film/substrate. The in-plane stresses in thin film – thick substrate systems typically arise from the combination of CTE and lattice mismatches. The Al_2O_3 film is not expected to crystallize in an epitaxial fashion on Si (100) [5]. Therefore, one would expect the CTE mismatch to contribute most of the stress. The film and the

ACCEPTED MANUSCRIPT

top of the Si substrate are proposed to be in high compressive stress in-plane that shifts the XRD peaks of the film ($20\bar{1}$) and the substrate (002) towards the lower degrees due to lattice expansion out-of-plane. The considerably high stress of the whole film-substrate system is also visible in Figure 4 where the measured curvature of the 10^5 Pa N_2 atmosphere sample is five times higher compared to the other experiments. The 10^5 Pa N_2 atmosphere samples Alumina 1 and 5, i.e., the complete wafers with the films, were also visually observed to be extremely crooked after the annealing treatments.

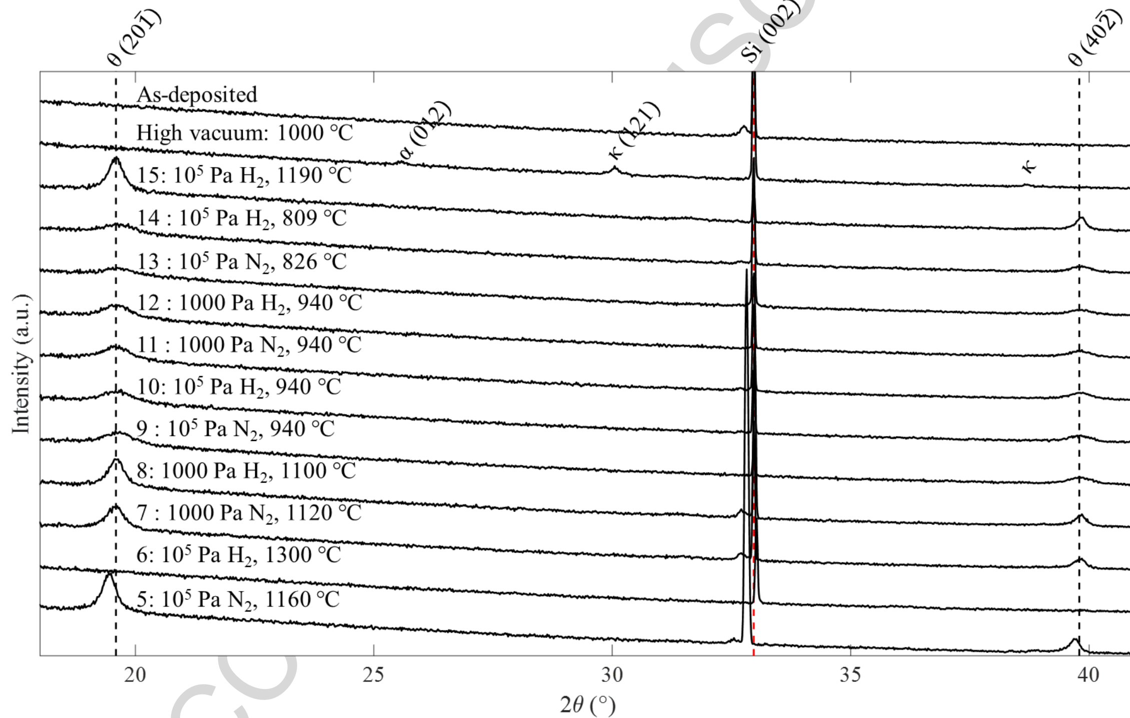

FIG 9. X-ray diffractograms of the films Alumina 5–15, high-vacuum-annealed, and as-deposited. The vertical, red, dashed line represents the Si (002) reflection. The peak before the Si (002) reflection was present in all the samples except for film 6 (drastically changed visual appearance) and HV. The manifestation of the aforementioned peak was spurious and also present in the as-deposited sample which is why it is not attributed to a crystalline phase of alumina. The θ , α and

ACCEPTED MANUSCRIPT

κ indexing were extracted from the ICSD utilizing References [30], [31] and [32] respectively. The comparative powder spectra of various alumina phases can be found in the supplementary material of [5].

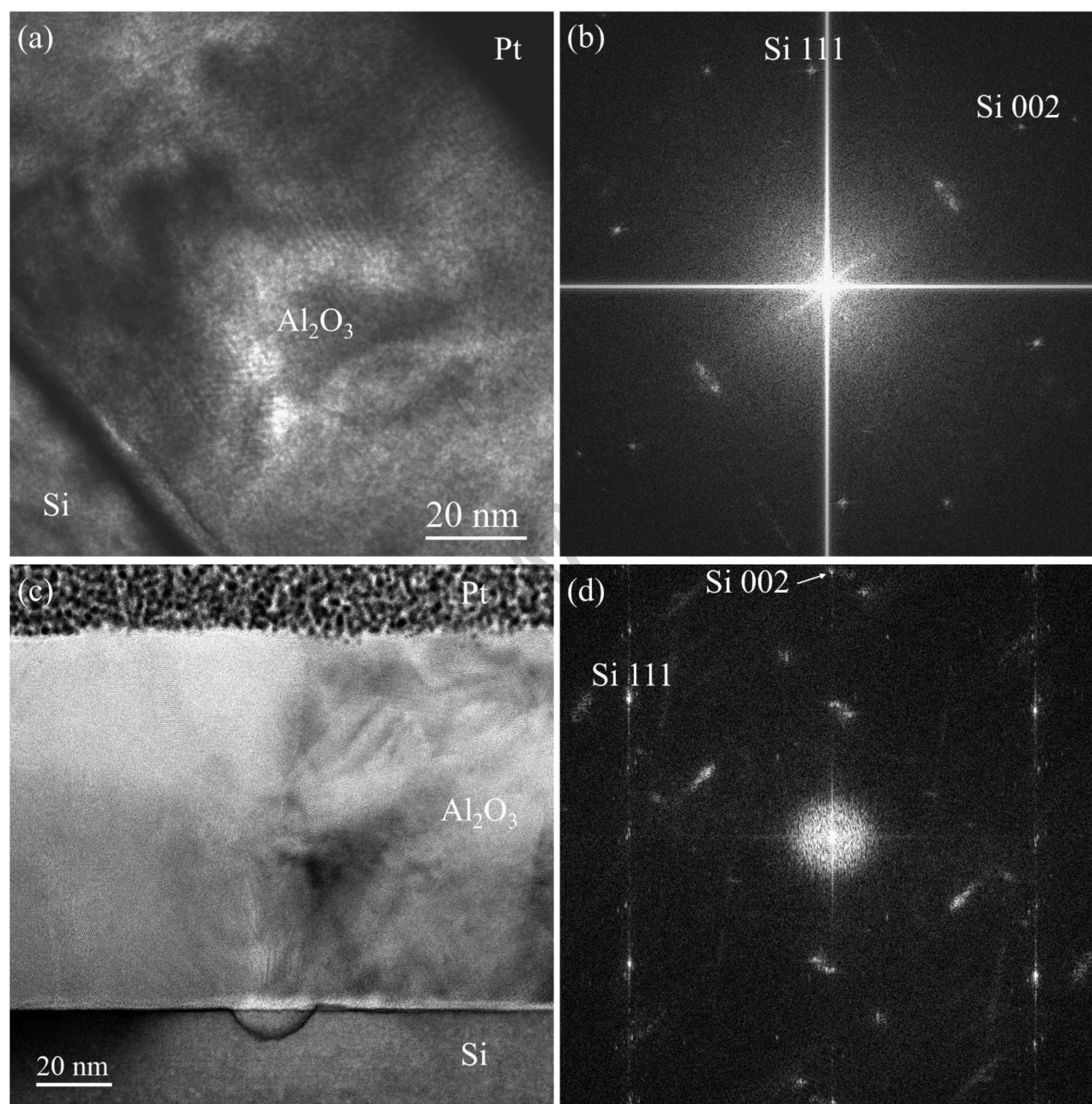

FIG 10. HRTEM images and their respective FFTs. (a)-(b) Al_2O_3 film annealed in N_2 at 1000 °C for one hour characterized in Ref. [5]. (c)-(d) Al_2O_3 film annealed in HV conditions at 1000 °C for one hour characterized in Ref. [29]. Both films were deposited with the same reactor and recipe but in a different batch from the ones characterized in this study. The images were taken along the

ACCEPTED MANUSCRIPT

Si <1$\bar{1}$0> zone axis. The cavity on Si in (c) is associated with blister formation investigated in [29].

The chemical compositions of films Alumina 5, 6, 11, and HV-annealed were investigated with ToF-ERDA depth profiling. Figure 11 presents the depth profiles and Table 3 the overall chemical compositions within the midsections of the films.

ACCEPTED MANUSCRIPT

ACCEPTED MANUSCRIPT

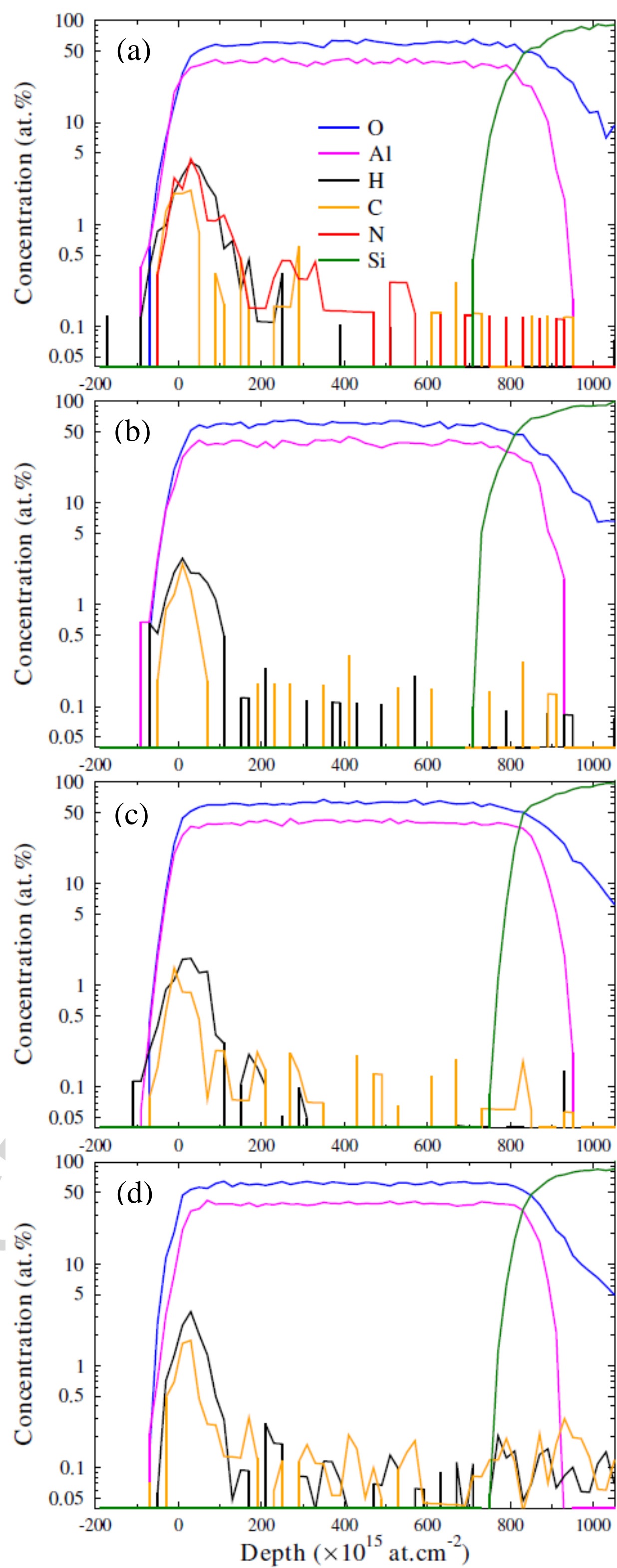

ACCEPTED MANUSCRIPT

FIG 11. ToF-ERDA depth profiles. (a) Alumina 5, 10^5 Pa N_2-annealed at 1160 °C (high stress). (b) Alumina 6, 10^5 Pa H_2-annealed at 1300 °C (white film). (c) Alumina 11, 1000 Pa N_2-annealed at 940 °C. (d) HV-annealed at 1000 °C from a different set of experiment with identical ALD deposition parameters and high vacuum annealing conditions as in this study.

TABLE 3. ERDA elemental compositions of annealed alumina films. Alumina HV is from a different deposition batch with identical ALD deposition parameters and high vacuum annealing conditions as in this study.

Sample	Al (at.%)	O (at.%)	H (at.%)	C (at.%)	N (at.%)
Alumina 5	40 ± 1	60 ± 2	< 0.05	< 0.05	0.20 ± 0.04
Alumina 6	39 ± 1	61 ± 2	< 0.05	< 0.05	0.20 ± 0.04
Alumina 11	40 ± 1	60 ± 2	0.06 ± 0.02	< 0.05	0.12 ± 0.02
Alumina HV	39 ± 1	61 ± 2	0.07 ± 0.03	0.08 ± 0.03	< 0.05

The ERDA depth profiles and elemental compositions (as-deposited in Figure 2, annealed in Figure 11 and Table 3) show that all films retain their as-deposited stoichiometry and loose impurities (H and C) in the bulk. The hydrogen and carbon impurities are mainly concentrated at the film surface in all cases, which is expected as the films were exposed to humid air conditions before ERDA measurements. Furthermore, Figure 11a of the film annealed in the 10^5-Pa N_2 atmosphere at 1160 °C shows nitridation at the surface. The nitridation has not had a marked effect on the surface hydrogen and carbon concentrations compared to the films without the nitridated

ACCEPTED MANUSCRIPT

surface. Finally, Alumina 6 – the film annealed in 10^5-Pa H_2 at 1300 °C – shows approximately stoichiometric Al_2O_3 despite the film had drastically changed its color and did not show alumina XRD peaks. Zhang et al.[17] have made a similar observation of ALD alumina losing its crystallinity after 1200 °C annealing. The drastic change in the color of films Alumina 2 and 6 is also clearly visible in the reflectance data of Figure 3 at 1300 °C.

4. DISCUSSION AND CONCLUSIONS

ALD alumina was annealed in various atmospheres at high temperatures up to 1300 °C. The annealing experiments included in-situ monitoring of the surface reflectance and wafer curvature. The surface reflectance data was used to evaluate the crystallization temperature of the films which was around 850 °C at the heating ramp rate of 0.2 °C/s, whereas delayed crystallization took place at 810 °C after a 15-minute incubation time. In addition, the crystallization of the same films has been demonstrated at 800 °C also, albeit these films showed a considerable amount of amorphous regions embedded in the films [5]. The in-situ reflectance data can be used to find crystallization kinetic parameters such as the incubation time and peak crystallization temperature of different ramp rates. It may be possible to find also the crystallized fraction but would require more experiments to understand the relationship between the reflectance and the crystallizing film.

The alumina films exhibited cracking above 1100 °C annealing. The cracks likely arose from thermomechanical stresses originating from the differences of the thermal coefficients of expansion between alumina and silicon. The cracks were observed visually and Figure 4 also showed discontinuities in the wafer curvature data towards the higher temperatures. The gradual increase in the wafer curvature in Figure 4 means that the thermomechanical stresses gradually built up until cracking occurred to relax the stresses. The cracking temperature imposes an absolute

ACCEPTED MANUSCRIPT

ACCEPTED MANUSCRIPT

upper limit for the annealing of ALD Al_2O_3 on Si (100) substrates, which is below 1100 °C, depending on the atmosphere. It should be noted that higher temperatures (1150 °C in N_2 demonstrated in [17]) can be possible with other substrates such as Si (111). In [17] the films were annealed with rapid thermal processing which may also affect the thermomechanical stresses. Furthermore, the 10^5 Pa N_2 annealing caused much higher wafer curvature than the other atmospheres. The nitradation of the surface, visible in the ToF-ERDA depth profile in Figure 11a, likely plays a role in the observed wafer curvature and XRD peak shift as no other difference in the film was detected compared to the other similar films.

The different atmospheres were selected to investigate the phase stabilities of the crystallizing alumina films since annealing in flowing nitrogen and in high vacuum had showed the films to crystallize in different phases or a mixture of phases.[5,29] Indeed, high vacuum annealing produced films with a mixture of θ, κ, and α phases while annealing in the other atmospheres produced only the θ phase. The substrates and the as-deposited films were identical in all of the annealing experiments. Therefore, the atmosphere likely plays a role in the phase stabilities either through heterogeneous nucleation originating from the surface of the film or via phase transformations during the annealing. The films that displayed only the θ phase did not transform to the α phase which would be expected to be the most stable phase [33], while the high-vacuum-annealed films showed a mixture of phases. Doping-related stabilization of the different phases is unlikely as the ERDA data did not show heavy elements associated with alumina phase stabilization modification [34]. In fact, ERDA did not show significant differences in composition between as-deposited and annealed films besides the removal of hydrogen and carbon. The stability of the θ phase, until the crystalline structure collapsed at around 1300 °C, can be explained by the dominant role of the surface energy in fine-grained thin films, which can alter the relative

ACCEPTED MANUSCRIPT

phase stabilities compared to bulk material [35,36]. The high vacuum seems to alter the surface energy of the film which can then either crystallize into a mixture of phases or later phase transform during the anneal via surface-assisted heterogeneous nucleation. Furthermore, the relative phase stabilities of nano-scale Al_2O_3 can be also altered by selecting a nano-sized substrate as demonstrated by the deposition of crystalline ALD alumina on nanowires at 200 °C [37].

It is unclear whether the high-vacuum-annealed films would have transformed completely to one of the three phases (θ, κ, or α) if the dwell time or temperature would have been increased. The annealing time in the high vacuum conditions was one hour contrary to a steady ramp in the MOVPE annealing max temperature experiments. Albeit, the ramp rate was only 0.2 °C/s in all the MOVPE experiments. It follows that the manifestation of the different phases could be due to kinetics. However, films 1–8 and 15 reached temperatures well above 1000 °C. As the phase transformations likely exhibit Arrhenius-type behavior (transformation rates exponentially commensurate to the temperature), it would be reasonable to assume that similar phase transformations would be seen if they would be purely temperature activated. The atmosphere hence plays a role in the transformation behavior.

A practical set of boundary conditions was identified for crystallizing ALD alumina via high-temperature treatments. The boundary conditions define alumina films crystallized in the θ phase that do not show blistering or cracks, and are chemically stable in the common wafer cleaning solutions. Furthermore, wafer curvature indicated nitrogen-annealing to induce unexpected warpage in the wafer-film combination whose origin was not clearly identified and require more studies. Finally, in-situ reflectance measurements were shown to be capable of gathering insight for crystallization kinetics investigations.

ACCEPTED MANUSCRIPT

ACCEPTED MANUSCRIPT

ACKOWLEDGEMENTS

The research was supported by ECSEL2014-2-662155 project: Informed, the Finnish Centre of Excellence in Nuclear and Accelerator Based Physics (Reference No. 251353) of the Academy of Finland, and the Academy of Finland Grant 297916. The research was conducted in the facilities of OtaNano, Aalto University and the University of Jyväskylä. Al_2O_3 deposition was carried out at Beneq Oy. Wafers were provided by Okmetic Oy.

[1] V. Miikkulainen, M. Leskelä, M. Ritala, R.L. Puurunen, Crystallinity of inorganic films grown by atomic layer deposition: Overview and general trends, J. Appl. Phys. 113 (2013) 21301. doi:10.1063/1.4757907.

[2] A. Pyymaki Perros, Thermal and plasma-enhanced atomic layer deposition: the study of and employment in various nanotechnology applications, Doctoral Thesis, Aalto University (2015) 57–58.

[3] P.D. Kirsch, M.A. Quevedo-Lopez, S.A. Krishnan, B.H. Lee, G. Pant, M.J. Kim, R.M. Wallace, B.E. Gnade, Mobility and charge trapping comparison for crystalline and amorphous HfON and HfSiON gate dielectrics, Appl. Phys. Lett. 89 (2006) 2–5. doi:10.1063/1.2392992.

[4] M. Broas, P. Sippola, T. Sajavaara, V. Vuorinen, A. Pyymaki Perros, H. Lipsanen, M. Paulasto-Kröckel, Structural and chemical analysis of annealed plasma-enhanced atomic layer deposition aluminum nitride films, J. Vac. Sci. Technol. A Vacuum, Surfaces, Film. 34 (2016) 41506.

ACCEPTED MANUSCRIPT

[5] M. Broas, O. Kanninen, V. Vuorinen, M. Tilli, M. Paulasto-Kröckel, Chemically Stable Atomic-Layer-Deposited Al2O3 Films for Processability, ACS Omega. 2 (2017) 3390–3398.

[6] D. Triyoso, R. Liu, D. Roan, M. Ramon, N. V. Edwards, R. Gregory, D. Werho, J. Kulik, G. Tam, E. Irwin, X.-D. Wang, L.B. La, C. Hobbs, R. Garcia, J. Baker, B.E. White, P. Tobin, Impact of Deposition and Annealing Temperature on Material and Electrical Characteristics of ALD HfO2, J. Electrochem. Soc. 151 (2004) F220. doi:10.1149/1.1784821.

[7] H. Kim, A. Marshall, P.C. McIntyre, K.C. Saraswat, Crystallization kinetics and microstructure-dependent leakage current behavior of ultrathin HfO 2 dielectrics: In situ annealing studies, Appl. Phys. Lett. 84 (2004) 2064–2066. doi:10.1063/1.1667621.

[8] J. Robertson, R.M. Wallace, High-K materials and metal gates for CMOS applications, Mater. Sci. Eng. R Reports. 88 (2015) 1–41. doi:10.1016/j.mser.2014.11.001.

[9] G.C. Correa, B. Bao, N.C. Strandwitz, Chemical Stability of Titania and Alumina Thin Films Formed by Atomic Layer Deposition, ACS Appl. Mater. Interfaces. (2015) 14816–14820. doi:10.1021/acsami.5b03278.

[10] R.L. Puurunen, J. Saarilahti, H. Kattelus, Implementing ALD layers in MEMS processing, ECS Trans. 11 (2007) 3–14.

[11] V. Sammelselg, I. Netšipailo, A. Aidla, A. Tarre, L. Aarik, J. Asari, P. Ritslaid, J. Aarik, Chemical resistance of thin film materials based on metal oxides grown by atomic layer deposition, Thin Solid Films. 542 (2013) 219–224. doi:10.1016/j.tsf.2013.06.079.

ACCEPTED MANUSCRIPT

ACCEPTED MANUSCRIPT

[12] L.H. Kim, K. Kim, S. Park, Y.J. Jeong, H. Kim, D.S. Chung, S.H. Kim, C.E. Park, Al2O3 /TiO2 Nanolaminate Thin Film Encapsulation for Organic Thin Film Transistors via Plasma-Enhanced Atomic Layer Deposition, ACS Appl. Mater. Interfaces. 6 (2014) 6731–6738. doi:10.1021/am500458d.

[13] A.I. Abdulagatov, Y. Yan, J.R. Cooper, Y. Zhang, Z.M. Gibbs, A.S. Cavanagh, R.G. Yang, Y.C. Lee, S.M. George, Al_2O_3 and TiO_2 atomic layer deposition on copper for water corrosion resistance., ACS Appl. Mater. Interfaces. 3 (2011) 4593–601. doi:10.1021/am2009579.

[14] M.-Y. Ho, H. Gong, G.D. Wilk, B.W. Busch, M.L. Green, P.M. Voyles, D.A. Muller, M. Bude, W.H. Lin, A. See, M.E. Loomans, S.K. Lahiri, P.I. Räisänen, Morphology and crystallization kinetics in HfO2 thin films grown by atomic layer deposition, J. Appl. Phys. 93 (2003) 1477–1481. doi:10.1063/1.1534381.

[15] D. Biswas, A.K. Sinha, S. Chakraborty, Optimization of annealing temperature for high- κ -based gate oxides using differential scanning calorimetry, J. Vac. Sci. Technol. B Nanotechnol. Microelectron. 33 (2015) 052205. doi:10.1116/1.4929442.

[16] S. Jakschik, U. Schroeder, T. Hecht, M. Gutsche, H. Seidl, J.W. Bartha, Crystallization behavior of thin ALD-Al2O3 films, Thin Solid Films. 425 (2003) 216–220. doi:10.1016/S0040-6090(02)01262-2.

[17] L. Zhang, H.C. Jiang, C. Liu, J.W. Dong, P. Chow, Annealing of Al2O3 thin films prepared by atomic layer deposition, J. Phys. D. Appl. Phys. 40 (2007) 3707–3713. doi:10.1088/0022-3727/40/12/025.

ACCEPTED MANUSCRIPT

[18] L.G. Gosset, J. Damlencourt, O. Renault, D. Rouchon, P. Holliger, Interface and material characterization of thin Al2O3 layers deposited by ALD using TMA / H2O, J. Non-Cryst. Solids 303 (2002) 17-23. doi: 10.1016/S0022-3093(02)00958-4.

[19] J. Aarik, A. Kasikov, M. Kirm, S. Lange, T. Uustare, H. Mändar, Optical properties of crystalline Al2O3 thin films grown by atomic layer deposition, Opt. Mater. Appl. Proc. SPIE. 5946 (2005) 594601. doi:10.1117/12.639047.

[20] R.F. Klie, N.D. Browning, A.R. Chowdhuri, C.G. Takoudis, Analysis of ultrathin SiO2 interface layers in chemical vapor deposition of Al2O3 on Si by in situ scanning transmission electron microscopy, Appl. Phys. Lett. 83 (2003) 1187–1189. doi:10.1063/1.1597415.

[21] O. Schön, B. Schineller, M. Heuken, R. Beccard, Comparison of hydrogen and nitrogen as carrier gas for MOVPE growth of GaN, J. Cryst. Growth. 189 (1998) 335–339.

[22] R.X. Wang, C.D. Beling, S. Fung, A.B. Djurišic, C.C. Ling, S. Li, Influence of gaseous annealing environment on the properties of indium-tin-oxide thin films, J. Appl. Phys. 97 (2005) 033504. doi:10.1063/1.1834984.

[23] M. Laitinen, M. Rossi, J. Julin, T. Sajavaara, Time-of-flight--Energy spectrometer for elemental depth profiling - Jyväskylä design, Nucl. Instruments Methods Phys. Res. Sect. B Beam Interact. with Mater. Atoms. 337 (2014) 55–61.

[24] R.L. Puurunen, Surface chemistry of atomic layer deposition: A case study for the trimethylaluminum/water process, J. Appl. Phys. 97 (2005) 121301. doi:10.1063/1.1940727.

ACCEPTED MANUSCRIPT

ACCEPTED MANUSCRIPT

[25] S.D. Elliott, G. Scarel, C. Wiemer, M. Fanciulli, G. Pavia, Ozone-based atomic layer deposition of alumina from TMA-- Growth, morphology, and retention mechanism, Chem. Mater. 18 (2006) 3764–3773.

[26] R. Matero, A. Rahtu, M. Ritala, M. Leskelä, T. Sajavaara, Effect of water dose on the atomic layer deposition rate of oxide thin films, Thin Solid Films. 368 (2000) 1–7. doi:10.1016/S0040-6090(00)00890-7.

[27] O.M.E. Ylivaara, X. Liu, L. Kilpi, J. Lyytinen, D. Schneider, M. Laitinen, J. Julin, S. Ali, S. Sintonen, M. Berdova, E. Haimi, T. Sajavaara, H. Ronkainen, H. Lipsanen, J. Koskinen, S.P. Hannula, R.L. Puurunen, Aluminum oxide from trimethylaluminum and water by atomic layer deposition: The temperature dependence of residual stress, elastic modulus, hardness and adhesion, Thin Solid Films. 552 (2014) 124–135. doi:10.1016/j.tsf.2013.11.112.

[28] F. Brunner, A. Knauer, T. Schenk, M. Weyers, J.-T. Zettler, Quantitative analysis of in situ wafer bowing measurements for III-nitride growth on sapphire, J. Cryst. Growth. 310 (2008) 2432–2438.

[29] M. Broas, H. Jiang, A. Graff, T. Sajavaara, V. Vuorinen, M. Paulasto-Kröckel, Blistering mechanisms of atomic-layer-deposited AlN and Al2O3 films, Appl. Phys. Lett. 111 (2017) 141606. doi:10.1063/1.4994974.

[30] E. Husson, Y. Repelin, Structural studies of transition aluminas. Theta alumina, Eur. J. Solid State Inorg. Chem. 33 (1996) 1223–1231.

[31] D.E. Cox, A.R. Moodenbaugh, A.W. Sleight, H.Y. Chen, Structural refinement of neutron

ACCEPTED MANUSCRIPT

and X-ray data by the Rietveld method: application to A1203 and BiV04, in: Accuracy in Powder Diffraction: Proceedings of a Symposium on Accuracy in Powder Diffraction Held at the National Bureau of Standards, Gaithersburg, Maryland, June, 11-15, 1979, 1980: p. 189.

[32] B. Ollivier, R. Retoux, P. Lacorre, D. Massiot, G. Férey, Crystal structure of κ-alumina: an X-ray powder diffraction, TEM and NMR study, J. Mater. Chem. 7 (1997) 1049–1056.

[33] I. Levin, D. Brandon, Metastable Alumina Polymorphs: Crystal Structures and Transition Sequences, J. Am. Ceram. Soc. 81 (2005) 1995–2012. doi:10.1111/j.1151-2916.1998.tb02581.x.

[34] J.M. Andersson, Controlling the formation and stability of alumina phases, Doctoral Thesis, Linköping University, 2005.

[35] J.M. McHale, A. Auroux, A.J. Perrotta, A. Navrotsky, Surface energies and thermodynamic phase stability in nanocrystalline aluminas, Science 80 (1997) 788–789. doi:10.1126/science.277.5327.788.

[36] A.H. Tavakoli, P.S. Maram, S.J. Widgeon, J. Rufner, K. Van Benthem, S. Ushakov, S. Sen, A. Navrotsky, Amorphous alumina nanoparticles: Structure, surface energy, and thermodynamic phase stability, J. Phys. Chem. C. 117 (2013) 17123–17130. doi:10.1021/jp405820g.

[37] S.M. Prokes, M.B. Katz, M.E. Twigg, Growth of crystalline Al2O3 via thermal atomic layer deposition: Nanomaterial phase stabilization, APL Mater. 2 (2014) 032105. doi:10.1063/1.4868300.

ACCEPTED MANUSCRIPT

ACCEPTED MANUSCRIPT

ACCEPTED MANUSCRIPT

- Annealed amorphous ALD Al_2O_3 crystallizes into various transition phases
- The annealing atmosphere plays a significant role in the crystallization
- The α phase is not manifested in certain annealing atmospheres
- Defect-free crystallized films can be produced with the appropriate conditions

ACCEPTED MANUSCRIPT